Proceedings of GT2005
ASME Turbo Expo 2005: Power for Land, Sea and Air
June 6-9, 2005, Reno-Tahoe, Nevada, USA

GT2005-69100

Simulation of Film Cooling Enhancement with Mist Injection

Xianchang Li and Ting Wang
Energy Conversion & Conservation Center
University of New Orleans
New Orleans, LA 70148-2220

Abstract

Cooling of gas turbine hot section components such as combustor liners, combustor transition pieces, turbine vanes (nozzles) and blades (buckets) is a critical task for improving the life and reliability of hot-section components. Conventional cooling techniques using air-film cooling, impingement jet cooling, and turbulators have significantly contributed to cooling enhancements in the past. However, the increased net benefits that can be continuously harnessed by using these conventional cooling techniques seem to be incremental and are about to approach their limit. Therefore, new cooling techniques are essential for surpassing these current limits. This paper investigates the potential of film cooling enhancement by injecting mist into the coolant. The computational results show that a small amount of injection (2% of the coolant flow rate) can enhance the cooling effectiveness about 30% ~ 50%. The cooling enhancement takes place more strongly in the downstream region, where the single-phase film cooling becomes less powerful. Three different holes are used in this study including a 2-D slot, a round hole, and a fan-shaped diffusion hole. A comprehensive study is performed on the effect of flue gas temperature, blowing angle, blowing ratio, mist injection rate, and droplet size on the cooling effectiveness with 2-D cases. Analysis on droplet history (trajectory and size) is undertaken to interpret the mechanism of droplet dynamics.

Keywords: film cooling, turbine blade cooling, mist cooling

Nomenclature

b	slot width (m)
C	concentration (kg/m^3)
c_p	specific heat (J/kg-K)
D	mass diffusion coefficient (m^2/s)
d	diameter (m)
F	force (N)
k	turbulence kinetic energy (m^2/s^2)
k_c	mass transfer coefficient (m/s)
h	convective heat transfer coefficient (W/m^2-K)
h_{fg}	latent heat (J/kg)
M	blowing ratio, $(\rho u)_c/(\rho u)_g$
m	mass (kg)
Nu	Nusselt number, hd/λ
P	pressure (N/m^2)
Pr	Prandtl number, ν/α
Re	Reynolds number, ud/ν
S	source term
Sc	Schmidt number (ν/D)
Sh	Sherwood number ($k_c d/D$)
T	temperature (K, ^oF)
t	time (s)
u	streamwise velocity component (m/s)
v	spanwise velocity component (m/s)
x, y, z	coordinates

Greek

α	thermal diffusivity (m^2/s)
ε	turbulence dissipation rate (m^2/s^3)
η	film cooling effectiveness, $(T_g-T_c)/(T_g-T_{aw})$
λ	heat conductivity (W/m-K)
μ	dynamic viscosity (kg/m-s)
ν	kinematic viscosity (m^2/s)
ρ	density (kg/m^3)
τ	stress tensor ($kg/m\text{-}s^2$)

Subscript

aw	adiabatic wall
c	coolant or jet flow
g	hot gas/air
p	particle or droplet
t	turbulent
0	values for air film cooling without mist
∞	values far away from droplets

Introduction

Cooling of gas turbine hot section components such as combustor liners, combustor transition pieces, turbine vanes (nozzles) and blades (buckets) has always been a critical task for improving the life and reliability of hot-section components. Air-film cooling has widely been used and intensively studied as an effective scheme for more than

half a century [1-2]. To improve the performance of air film cooling, many studies have been conducted by examining the effect of flow and geometric parameters, including injection angles, injection hole configuration, density ratio and blowing ratio. For example, Jia, et al. [3] investigated a slot jet film cooling by using numerical simulations coupled with LDV experiments. Different jet angles from 15 to 60 degrees with jet-blowing ratios ranging from 2 to 9 were studied. Their results showed a recirculation bubble downstream the jet vanishes when the angle is 30 degrees or less. They also found the blowing ratio has a large effect on the size of recirculation, and consequently on film cooling. Kwak and Han [4] measured heat transfer coefficients and film-cooling effectiveness on a gas turbine blade tip. Their results showed as blowing ratio increased, heat transfer coefficient decreased while film effectiveness increased. Heat transfer coefficient and film effectiveness were found to increase with increasing tip gap clearance. Wang, et al. [5] conducted an experimental study focusing on the flow mixing behavior inside the slots. Various parameters including orientation angle, inclination angle, slot width, effect of primary flow and slot depth were systematically examined. The optimum slot depth was found to range from 2 to 2.8 times the jet diameter. The compound angle configuration (60° jet orientation and 30° slot inclination angles) was discovered to be the best choice.

Among the typical holes are simple-angle holes with lateral or forward diffusion and compound-angle holes with forward diffusion. The performance of film cooling with different holes varies by 30~50% subject to geometric and flow conditions. Bell et al. [6] studied film cooling from shaped holes and measured the local and spatially averaged adiabatic film cooling effectiveness. They found laterally diffused, compound angle holes and forward diffused and compound angle holes produce higher effectiveness magnitudes over much wider ranges of blowing ratio and momentum flux ratio compared to the other three simple-angle configurations tested. All the three simple angle hole geometries (cylindrical round, simple angle holes, laterally diffused, simple angle holes, and forward diffused, simple angle holes, show larger increases of spanwise-averaged adiabatic effectiveness as the density ratio increases from 0.9 to 1.4. Brittingham and Leylek [7] performed numerical simulation on film cooling with compound-angle shaped holes and concluded that superposition of individual effects for compound-angle cylindrical holes and streamwise shaped holes do not necessarily apply to compound-angle shaped holes. The compound-angle shaped holes can be designed to eliminate crossflow line-of-sight between adjacent holes, and thus somewhat mimic slot-jet performance. From many of the previous studies, the optimal blowing ratio is discovered ranging from 0.5 to 1.0. The 35-degree injection angle and the shaped-holes are found to be the most effective.

As next generation turbines will be required to burn alternate fuels with high hydrogen (H_2) and carbon monoxide (CO) content from coal-derived syngas, cooling gas turbines becomes more difficult and more important. The high contents of H_2 and CO will increase flame temperatures and flame speeds from those of natural gas combustion. Although conventional cooling techniques using air-film cooling, impingement jet cooling, and turbulators have significantly contributed to cooling enhancements in the past, the increased net benefits, which can be continuously harnessed by using these conventional cooling techniques, seem to be incremental and are about to approach their limit. Therefore, new cooling techniques are essential. This paper investigates the potential of film cooling enhancement by injecting mist into the coolant. Film cooling with mist injection can improve single-phase air film cooling due to the following mechanisms: (a) the latent heat of evaporation serves as a heat sink to absorb large amounts of heat; (b) direct contact of liquid droplets with the cooling wall can significantly increase heat transfer from wall; (c) steam and water have higher specific heats (c_p) than air. In a single-phase air-cooling, film cooling becomes less and less effective as it moves into the downstream region. By taking advantage of the residence time needed to evaporate tiny water droplets, mist can also be strategically used to blanket weakened air-cooling in the downstream region. Significant enhancement of film cooling can reduce the cooling air and thus lower the pressure drop.

Mist has been used to enhance heat transfer in gas turbine systems in many different ways. A well-known application is gas turbine inlet air fog cooling [8], in which the droplets evaporate to lower the air inlet temperature until the relative humidity reaches 100%. In addition, fog overspray is used in industry to provide cooling in the compressor. Petr [9] shows the results of thermodynamic analysis of the gas turbine cycle with wet compression based on detailed simulation of a two-phase compression process. In 1998, Nirmalan et al. [10] applied water/air mixture as the impingement coolant to cool gas turbine vanes. They used an airfoil containing a standard impingement tube that distributes the water-air mixture over the inner surface of the airfoil. The water flash vaporizes off the airfoil inner wall and very high cooling rates were achieved. To explore an innovative approach to cool future high-temperature gas turbines, Guo et al. [11] studied the mist/steam cooling in a heated straight tube by injecting 7 μm (average diameter) of water droplets into the steam flow. The highest local heat transfer enhancement of 200% was achieved with 1~5% (weight) mist, and the average enhancement was 100%. Guo et al. [12] also conduced mist/steam cooling study in a 180^o tube bend. The overall cooling enhancement ranged from 40% to 300% with the maximum local cooling enhancement being over 800%, which occurred at about 45^o downstream of the inlet of the test section. Li et al. [13] reported results of mist/steam cooling with a slot jet on a heated flat surface. Their results showed a 200% cooling enhancement near the stagnation point by adding 1.5% mist (in mass) to the steam flow. The mist enhancement declined to near zero by five slot widths downstream. Li et al. [14] also investigated mist/steam slot jet impinging on a concave surface. Enhancements of 30 to 200% were achieved within five slot distance by adding 0.5% (weight) mist.

Injecting water mist into film cooling flow has not been favored by gas turbine manufacturers due to concerns on potential erosion and corrosion problems on turbine airfoils. However, the current concern, from the point of practical applications, should not hinder the exploration of new ideas that may provide an attractive reward. The objective of this study is to initiate a preliminary investigation on whether there is potential merit in injecting mist into film cooling flow. A numerical simulation is performed in this paper. Three different holes are used in this study including a 2-D slot, a round hole, and a diffusion hole. The computational results show that a small amount of injection (2% of the coolant flow rate) can significantly increase the cooling effectiveness up to 50%. A comprehensive investigation is also given to the effect of mainstream temperature, blowing angle, blowing ratio, mist injection rate, and droplet size on the cooling effectiveness. The adiabatic film cooling effectiveness is compared for different cases.

Numerical Model

To study the mist effect on air film cooling, a 2-D slot is first used in this study. As shown in Fig. 1, the slot width (b) is 4 mm. The computational domain has a length of 80b and a height of 20b. The slot jet is set to 20b from the entrance of mainstream. The injection angle is 35 degrees, which is considered as the optimal value [6, 7]. A

smaller angle (30 degrees) is also examined. The vertical height of the jet hole is 1.74b, which gives an actual jet hole length of 3.04b. Notice that the length of jet holes as well as the settling chamber before the jet holes can affect the numerical results of film cooling. Since this study focuses on air-film cooling using the mist effect, the upstream condition of coolant in the chamber is not included. Two 3-D holes are adopted to investigate the effect of mist transport encountering the 3-D effect: one is a round hole with a simple blowing angle of 35 degrees, and the other is a fan-shaped hole with the same blowing angle. Both holes have a diameter (d) of 8 mm, and the lateral diffusion angle of the fan-shaped hole is 12 degrees, which is the same as reported in [6-7]. Other different diffusion angles, for example in [15], are not investigated in this study. The length and width of the 3-D domain are kept the same as the slot hole case, and the depth of the domain is 4d, as shown in Fig. 1b.

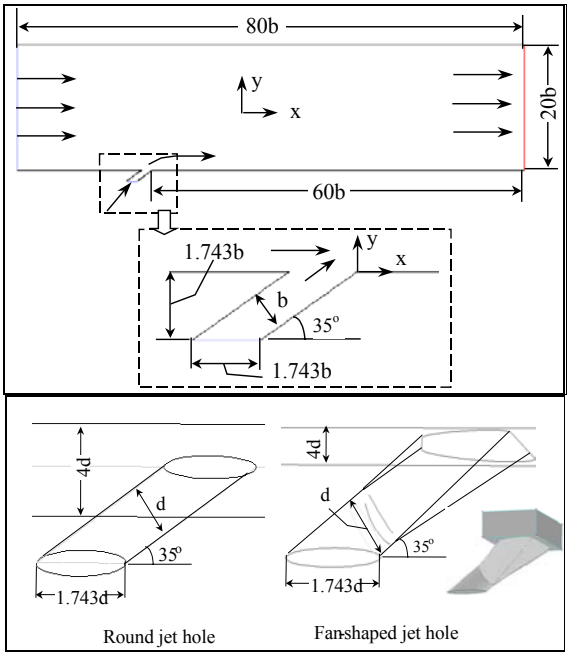

Figure 1 Computational Domain and Film Hole Configurations

The commercial software package Fluent (version 6.1.22) from Fluent, Inc. is used in this study. The simulation uses the segregated solver, which employs an implicit pressure-correction scheme [16]. The SIMPLE algorithm is used to couple the pressure and velocity. Second order upwind scheme is used for spatial discretization of the convective terms and species. In Fluent, the Lagrangian trajectory calculations were employed to model the dispersed phase of particles, droplets or bubbles, including coupling with the continuous phase. The impact of the droplets on the continuous phase is considered as source terms to the governing equations. After obtaining an approximate flow field of the continuous phase (airflow in this study), Fluent traces the droplet trajectories, and computes heat and mass transfer between the droplets and the airflow.

Continuous Phase (Air/Steam)

Governing Equations – The standard 2-D/3-D, time-averaged, steady-state Navier-Stokes equations as well as equations for mass, energy and species transport are solved. The governing equations for conservation of mass, momentum, and energy can be given as:

$$\frac{\partial}{\partial x_i}(\rho u_i) = S_m \tag{1}$$

$$\frac{\partial}{\partial x_i}(\rho u_i u_j) = \rho \vec{g}_j - \frac{\partial P}{\partial x_j} + \frac{\partial \tau_{ij}}{\partial x_i} + F_j \tag{2}$$

$$\frac{\partial}{\partial x_i}(\rho c_p u_i T) = \frac{\partial}{\partial x_i}\left(\lambda_{eff}\frac{\partial T}{\partial x_i}\right) + \mu\Phi + S_h \tag{3}$$

where the source terms (S_m, F_j and S_h) are used to include the contributions from the dispersed phase. τ_{ij} is the symmetric stress tensor, which can be expressed as

$$\tau_{ij} = \mu\left(\frac{\partial u_j}{\partial x_i} + \frac{\partial u_i}{\partial x_j} - \frac{2}{3}\delta_{ij}\frac{\partial u_k}{\partial x_k}\right). \tag{4}$$

$\mu\Phi$ is the heat of dissipation and λ_{eff} is the effective heat conductivity. When turbulence effect is considered, both τ_{ij} and λ_{eff} need to be modeled.

Since evaporation of droplets releases water vapor into the main airflow, species transport needs to be considered. There are 3 species considered, water vapor (H_2O), Oxygen (O_2) and Nitrogen (N_2), and dry airflow is simulated as 23% O_2 and 77 N_2 by mass. The equation for species transport is

$$\frac{\partial}{\partial x_i}(\rho u_i C_j) = \frac{\partial}{\partial x_i}\left(\rho D_{eff,j}\frac{\partial C_j}{\partial x_i}\right) + S_j, \tag{5}$$

where C_j is the mass fraction of one of the species (j) in the mixture, and S_j is the source term for this species. $D_{eff,\,j}$ is the effective diffusion coefficient considering the turbulence effect.

Turbulence Model - The main flow in this study has a velocity of 10 m/s, which gives a passage Reynolds number of 40,000. Therefore, turbulence model must be considered. The interaction between the injected flow and the approaching flow could be anisotropic and nonequilibrium with multiscaled integral and dissipation length scales. Since the focus of this paper is not searching for a better turbulence model to account for the anisotropic turbulence structure, the effect of turbulence models on the computational results are not investigated. Comparing the current study with the existing literature shows the standard k-ε with enhanced wall treatment is one of the robust turbulence models for film cooling flow, thus the standard k-ε model is used in this study. The equations for the turbulent kinetic energy (k) and its dissipation rate (ε) are:

$$\frac{\partial}{\partial x_i}(\rho u_i k) = \frac{\partial}{\partial x_i}\left[\left(\mu + \frac{\mu_t}{\sigma_k}\right)\frac{\partial k}{\partial x_i}\right] + G_k - \rho\varepsilon. \tag{6}$$

$$\frac{\partial}{\partial x_i}(\rho u_i \varepsilon) = \frac{\partial}{\partial x_i}\left[\left(\mu + \frac{\mu_t}{\sigma_\varepsilon}\right)\frac{\partial \varepsilon}{\partial x_i}\right] + C_{1\varepsilon}G_k\frac{\varepsilon}{k} - C_{2\varepsilon}\rho\frac{\varepsilon^2}{k}. \tag{7}$$

The term G_k is the generation of turbulence kinetic energy due to the mean velocity gradients. The turbulent viscosity, μ_t, is calculated from the equation

$$\mu_t = \rho C_\mu \frac{k^2}{\varepsilon} \tag{8}$$

and the effective heat conductivity (λ_{eff}) and the effective diffusion coefficient are calculated by the following two equations, respectively.

$$\lambda_{eff} = \lambda + c_p\mu_t / Pr_t, \tag{9}$$

$$D_{eff} = D + \mu_t / Sc_t \ . \quad (10)$$

The constants $C_{1\varepsilon}$, $C_{2\varepsilon}$, C_μ, σ_k, and σ_ε used are: $C_{1\varepsilon} = 1.44$, $C_{2\varepsilon} = 1.92$, $C_\mu = 0.09$, $\sigma_k = 1.0$, $\sigma_\varepsilon = 1.3$ [17]. The turbulence Prandtl number, Pr_t, is set to 0.85, and the turbulence Schmidt number, Sc_t, is set to 0.7. The equations may include more other source terms, for example, turbulence kinetic energy due to buoyancy and the contribution of fluctuating dilatation in compressible turbulence.

In the enhanced wall treatment, the standard two-layer model is combined with wall functions. To apply the two-layer approach, the computational domain is separated into a viscosity-affected region and a fully-turbulent region by defining a turbulent Reynolds number, Re_y, which is based on the distance from the wall.

$$Re_y = yk^{1/2} / \nu \quad (11)$$

where k is the turbulence kinetic energy and y is the distance from the wall. The flow is assumed in the fully turbulent region if $Re_y > 200$, and the k-ε model is used. Otherwise, the flow is in the viscosity-affected region, and the one-equation model of Wolfstein [18] is used. The turbulent viscosities calculated from the two regions are blended with a blending function (θ) to make the transition smooth.

$$\mu_{t,enhanced} = \theta\mu_t + (1-\theta)\mu_{t,l} \quad (12)$$

where μ_t is the viscosity from the k-ε model of high Reynolds number, and $\mu_{t,l}$ is the viscosity from the near-wall one-equation model. The blending function is defined so it is 0 at the wall and 1 in the fully-turbulent region. The wall functions are also enhanced by blending linear (laminar) and logarithmic (turbulent) laws-of-the-wall to make the applicability throughout the entire near-wall region.

Boundary Conditions - The main flow is assumed to be dried air (zero humidity) and the jet flow is saturated air (100% relative humidity). Uniform velocity and temperature are assigned to the domain inlet and jet hole inlet. The mainstream velocity is 10 m/s, and its temperature is 400K. The jet velocity is also 10 m/s, and the temperature is 300K. Note that these parameters are referenced in many previous studies of air-film cooling, for example [6], although they are not corresponding to the real conditions in gas turbine applications. While the current paper serves as conceptual study on film cooling with mist injection, further research is to be performed with more realistic parameters for gas turbine application. To compare the results of this study to other published work, these values used by the previous published work are adopted in this study. To study the effect of mist under different blowing and temperature ratios, other values of the flow temperature and jet velocity are assigned. The inlet conditions of the turbulence are 1 m^2/s^2 for the turbulence kinetic energy and 1 m^2/s^3 for the dissipation rate, which is equivalent to a turbulent intensity of 1%. The flow exit (outlet) of main computational domain is assumed to have a constant pressure. The backflow (reverse flow), if any, is set to 400 K.

All the walls in the computational domain are adiabatic and have a non-slip boundary condition. Zero velocity and temperature gradients are assigned to the side boundaries of the 3-D computational domain (i.e. symmetric boundary condition).

Discrete Phase (Water Droplets)

Droplet Flow and Heat Transfer – Basically, the droplets in the airflow can encounter inertia and hydrodynamic drags. Because of the forces experienced by a droplet in a flow field, the droplet can be either accelerated or decelerated. The velocity change can be formulated by

$$d\mathbf{v_p}/dt = \mathbf{F_d} + \mathbf{F_g} + \mathbf{F_o} \quad (13)$$

where $\mathbf{F_d}$ is the drag of the fluid on the droplet and $\mathbf{F_g}$ is the gravity. $\mathbf{F_o}$ represents the other forces, and $\mathbf{v_p}$ is the droplet velocity (vector). Among the forces represented by F_o are typically included the "virtual mass" force, thermophoretic force, Brownian force, Saffman's lift force, etc.

Theoretically, evaporation occurs at two stages: (a) when temperature is higher than the saturation temperature (based on local water vapor concentration), water evaporates, and the evaporation is controlled by the water vapor partial pressure until 100% relative humidity is achieved; (b) when the boiling temperature (determined by the air-water mixture pressure) is reached, water continues to evaporate. After the droplet is evaporated due to either high temperature or low moisture partial pressure, the vapor diffuses into the main flow and is transported away. The rate of vaporization is governed by concentration difference between surface and air stream, and the corresponding mass change rate of the droplet can be given by,

$$\frac{dm_p}{dt} = \pi d^2 k_c (C_s - C_\infty) \quad (14)$$

where k_c is the mass transfer coefficient and C_s is the concentration of the vapor at the droplet surface, which is evaluated by assuming that the flow over the surface is saturated. C_∞ is the vapor concentration of the bulk flow, obtained by solving the transport equations. The values of k_c can be calculated from empirical correlations by [19-20]

$$Sh_d = \frac{k_c d}{D} = 2.0 + 0.6 Re_d^{0.5} Sc^{0.33} \quad (15)$$

where Sh is the Sherwood number, Sc is the Schmidt number (defined as ν/D), D is the diffusion coefficient of vapor in the bulk flow.

When the droplet temperature reaches the boiling point, the following equation can be used to evaluate its evaporation rate [21]:

$$\frac{dm_p}{dt} = \pi d^2 \left(\frac{\lambda}{d}\right)(2.0 + 0.46 Re_d^{0.5}) \ln\left(1 + c_p(T_\infty - T)/h_{fg}\right)/c_p \quad (16)$$

where λ is the heat conductivity of the gas/air, and h_{fg} is the droplet latent heat. c_p is the specific heat of the bulk flow.

The droplet temperature can also be changed due to heat transfer between droplets and the continuous phase. Without considering radiation heat transfer, the droplet's sensible heat change depends on the convective heat transfer and latent heat (h_{fg}), as shown in the following equation.

$$m_p c_p \frac{dT}{dt} = \pi d^2 h(T_\infty - T) + \frac{dm_p}{dt} h_{fg} \quad (17)$$

where the convective heat transfer coefficient (h) can be obtained with a similar empirical correlation to Eq. 15 [19-20]:

$$Nu_d = \frac{hd}{\lambda} = 2.0 + 0.6 Re_d^{0.5} Pr^{0.33} \quad (18)$$

where Nu is the Nusselt number, and Pr is the Prandtl number.

In mist film cooling, the temperature of main flow will be above the water boiling temperature. Notice the characteristic velocity in Re_d is the relative velocity between the droplet and airflow, which is usually small for droplets in micrometers. Therefore, Re_d is also very small. In addition, the term $c_p(T_\infty - T)/h_{fg}$ in Eq. 16 can be much smaller than 1 (0.04 in this study). By ignoring the term with Re and

using $\ln(1+\delta) = \delta$, the approximate droplet evaporation time can be obtained as:

$$t = \frac{h_{fg}\rho d^2}{2\lambda (T_\infty - T)} \tag{19}$$

It can be seen that the evaporation time is proportional to the square of diameter. Assuming d = 10 μm and T_∞ -T = 100K, the evaporation time will be 0.038 seconds. If the average velocity of droplets is 6 m/s, the distance to evaporate the droplets is 0.23 m. Considering the length of 0.24 m downstream of the slot in this study, this means theoretically most of the droplets less than 10 μm are expected to evaporate inside the computational domain; whereas, the droplets larger than 10 μm or at a higher speed will not evaporate within the computational domain. Lower temperature difference will lengthen the evaporation, but the neglected term means an even shorter time in reality.

Stochastic Particle Tracking - The effects of turbulence on the dispersion of droplets/particles is considered by using stochastic tracking. Basically, the droplet trajectories are calculated by using the instantaneous flow velocity ($\bar{u} + u'$) rather than the average velocity ($\bar{u}$). The velocity fluctuations are then given as:

$$u' = \varsigma\left(\overline{u'^2}\right)^{0.5} = \varsigma(2k/3)^{0.5} \tag{20}$$

where ζ is a normally distributed random number. This velocity will apply during the characteristic lifetime of the eddy (t_e), a time scale defined by either of the following equations:

$$t_e = 0.3k/\varepsilon \tag{21}$$

$$t_e = -0.15k/\varepsilon \log(r) \tag{22}$$

where r is a uniform distributed random number ranging from 0 to 1. In case the droplet slip velocity is so large that the time for the droplet to cross the eddy is shorter than the time defined above, the droplet eddy crossing time will be used, which is defined as:

$$t_{cross} = -t_p \ln[1 - L_e/(t_p \mid u - u_p \mid)] \tag{23}$$

where t_p is the particle relaxation time with $t_p = \rho_p d_p^2/(18\rho_g \nu_g)$, L_e is the eddy length scale, and $|u-u_p|$ is the magnitude of the relative velocity. After this time period, the instantaneous velocity will be updated with a new ζ value until a full trajectory is obtained. The random effect of the turbulence on the droplets can predicted reasonably only if a sufficient number of trajectories are calculated. In this study, the trajectory number is chosen to be 25 and several test runs indicated that increasing this number does not make the result much different.

Mist Injection and Droplet Sizes – For the 2-D slot case, the mist is injected at 25 locations uniformly distributed in the jet inlet. For 3-D holes, the injection is also uniform in the surface perpendicular to the hole centerline. The total number of injections is 904 for the round hole and 941 for the fan-shaped hole. The injection flow rate varies from 1 to 5% of the coolant air in mass. For example, considering the 2-D slot case with a depth of 1 meter, the droplets flow rate will be 3.5×10^{-4} to 1.75×10^{-3} kg/s. The injection rate at each location is 1.4×10^{-5} kg/s for 2% injection. It is known that the droplet size can strongly affect the evaporation of the mist in the main airflow. Uniform droplets with different sizes (5, 10, 20 and 50 μm) are used in this study to examine the effect on film cooling performance. Non-uniform droplets in real application are assumed to perform as a combination of droplet with different uniform sizes. The boundary condition of droplets at all the walls is assigned as "reflect", which means the droplets are elastically rebound off once reaching the wall. At the outlet, the droplets just simply flee/escape from the computational domain. A more complex model will be developed in the future to determine if the droplets breakup, rebound, or are trapped by the wall when they hit it.

Meshes and Convergence

Structured but non-uniform grids are used for the 2-D slot case in this study. The grids near the jet wall and the bottom wall of the main domain are denser than the other area. For the 3-D cases, un-structured grids are applied to the jet holes and a small volume in the main domain close to the jet outlet. Structured grids are used for the rest of domain. Figure 2 shows the grids of the 2-D case and some planes for 3-D cases. The grid number is 200 in the longitudinal (streamwise) direction and 60 in both the transverse y- and spanwise z-directions. There are 360,000 cells for the round-hole case and 386,000 cells for the fan-shaped hole case.

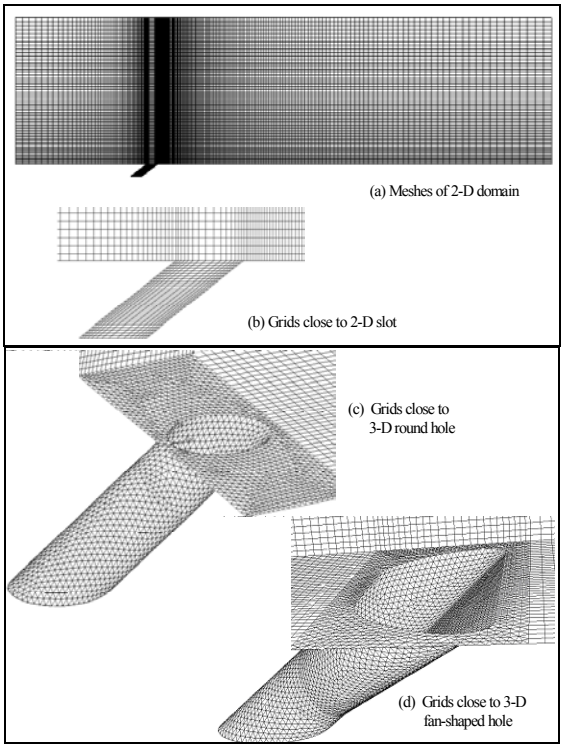

Figure 2 Meshes

Grid Independence Study - Different meshes have been tested for grid dependence. For example, the average cooling effectiveness (defined later) changes only 0.8% when the density of the 2-D mesh in Fig. 2 is doubled. Figure 3 shows the results of temperature and velocity profiles for a 2-D slot jet using different meshes. It can be seen that the difference due to the number of grids is small. Therefore, no finer grids are attempted.

Convergence - Converged results can be reached after iteration proceeds alternatively between the continuous and discrete phases. Ten iterations in the continuous phase are conducted between two iterations in the discrete phase. A typical converged result renders mass residual of 10^{-3}, energy residual of 10^{-6}, and momentum and

turbulence kinetic energy residuals of 10^{-4}. These residuals are the summation of the imbalance for each cell, scaled by a representative of the flow rate. Typically, 1000 to 2000 iterations are needed to obtain a converged result, which takes about 1~2 hours for a 2-D case and 10~20 hours for a 3-D case on a PC with Pentium 4 processor of 2.4 GHz.

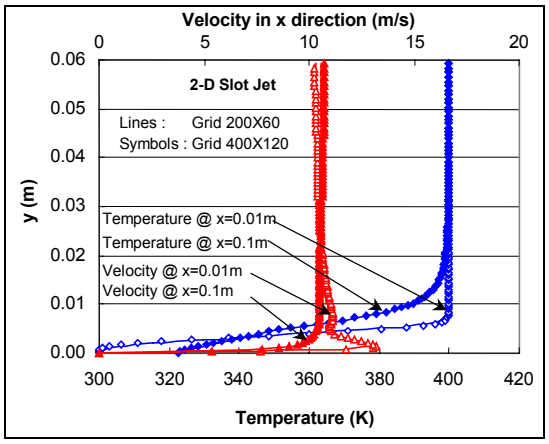

Figure 3 Grid Impendence Study (Slot jet)

Results and Discussion

As a reference case, the overall temperature distribution of film cooling with the 2-D slot is shown in Fig. 4, in which (a) is the case without mist and (b) is the case with 2% mist injection using 10-μm droplets. The temperatures of jet and main flow are 300K and 400K, respectively. The blowing ratio, defined as $M=(\rho u)_c/(\rho u)_g$, is 1.3 in this case, while the ratio of velocity is 1. Here the subscript "c" represents the coolant or jet flow, and the subscript "g" represents the main gas flow. The overall temperature distribution with mist is not much different from that of a typical air-film cooling. The cold jet sticks to the cooling surface but gradually becomes hot and diffuses to the main stream by shear layer mixing. It seems that the 2% mist injection has little effect on the overall temperature profile in the main flow. However, a detailed study can find that the temperature very close to the cooling surface decreases due to mist injection as shown in Fig. 5. The adiabatic wall temperature decreases about 9K downstream the jet at x=25b. Note that the origin of x-coordinate is set at the downstream end of the jet holes for both 2-D and 3-D cases. At the beginning of film cooling, the evaporation of droplets is negligible because of the low flow temperature.

The adiabatic cooling effectiveness (η) is used to examine the performance of mist film cooling. The definition of η is:

$$\eta = (T_g - T_{aw})/(T_g - T_c) \qquad (24)$$

where T_g is the mainstream hot gas temperature, T_c is the temperature of the coolant (jet), and T_{aw} is the adiabatic wall temperature. η is between zero (no cooling) and 1 (the wall temperature is the same as the coolant temperature). Figure 6 shows the effectiveness along the cooling surface. Note that 2b is used to scale the distance downstream because it is the hydraulic diameter of a slot. It can be seen that film cooling is significantly enhanced by mist injection, especially in the downstream region, where the evaporation of droplets becomes stronger because of the higher flow temperature. Due to continuous mixing between coolant and the main flow, the cooling inevitably becomes less effective downstream, and it has been a serious challenge to enhance cooling downstream of x/2b=15. The injection of water droplets works very well to meet this challenge. Also shown in Fig. 6 is the ratio of the film cooling effectiveness with and without mist (η_{mist}/η_0). The mist-cooling enhancement can be defined as (η_{mist}/η_0-1). It can be seen that the maximum enhancement can reach 38% further downstream (x/2b=30) with an average cooling enhancement of 14.5%.

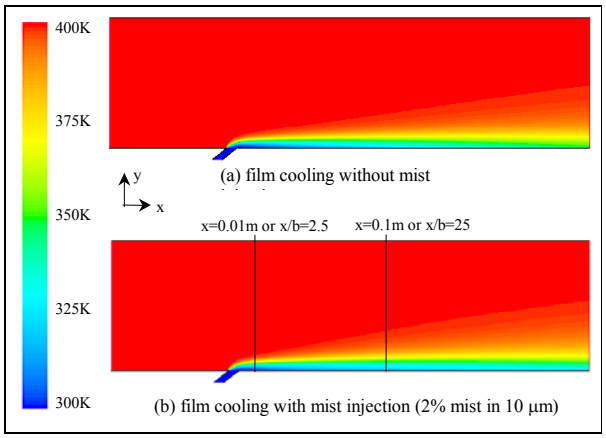

Figure 4 Temperature distribution of air-film cooling with and without mist injection (Slot jet)

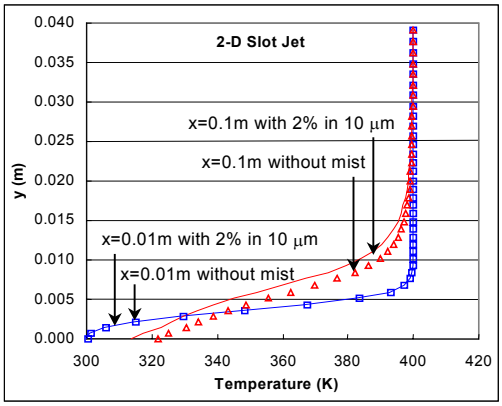

Figure 5 Effect of 2% mist injection on temperature distribution at different locations (Slot jet)

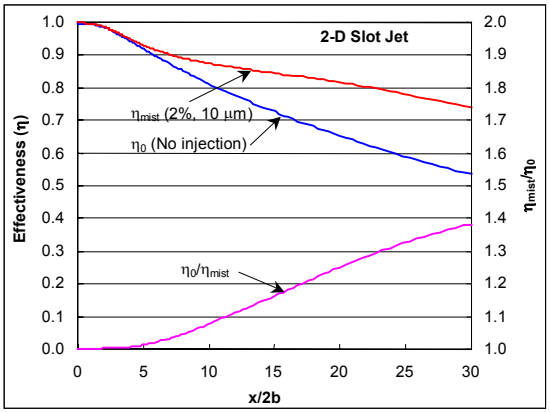

Figure 6 Effectiveness of film cooling and mist enhancement (2-D slot)

Mist Film Cooling with 3-D Injection Holes - While a slot hole is ideal to study fundamental characteristics of film cooling, 3-D holes are more practical due to mechanical structural and manufacturing considerations. A simple-angle round hole and a fan-shaped hole are studied. Figure 7 shows the results of temperature distributions on the cooling surface for both the round and fan-shaped holes. The mist injection is 2% of the mass of jet airflow. Both holes have the same inlet velocity and thus the same flow rate. It can be seen that the mist lowers the surface temperature in both cases. The fan-shaped hole produces a lower temperature than the round hole. More discussions will be given later.

The cooling effectiveness is given in Figs. 8 and 9 to examine the mist film cooling performance. For the round hole, the cooling effectiveness along the centerline drops sharply at the beginning within a 4d distance, and the effect of mist is small. Starting at about 4d downstream, the mist shows its strong contribution. The same trend can be seen for the cooling effectiveness averaged along the spanwise direction (z) except the averaged effectiveness has a minimum around x/d=5. The mist cooling enhancement of 2% is about 43% downstream (x/d = 30) with a maximum of 50% near x/d = 12. The effectiveness of the round hole is low when it is compared with the fan-shaped hole; therefore its enhancement is essential. Figure 9 shows the performance of film cooling with the fan-shaped hole. Compared to the round hole, the fan-shaped hole produces higher cooling effectiveness along the centerline and on spanwise average. The mist cooling enhancement is about the same as the round-hole case: 47% downstream (x/d = 30) with a maximum of 52%. However, the maximum enhancement moves to about x/d =18.

The different behaviors between the round hole and fan-shaped hole can be further analyzed with Figs. 10 and 11. Figure 10 shows the flow field and temperature distribution on a cross-section in the x-direction. It can be seen that the center of coolant jet from the round hole is detached away from the cooling surface, and the secondary flow of the round hole case is strong and entrains surrounding hot gas to the surface. These features reduce the blanket effect of the cooling layer. On the other hand, the fan-shaped hole can keep the jet center close to the surface, and the secondary flow is weak. It is expected that the evaporation of mist be strongly affected by the jet flow itself. The flow structure determines the cooling effectiveness along the z-direction. As shown in Fig. 11, the round hole gives a narrower spanwise film cooling coverage than the fan-shaped hole.

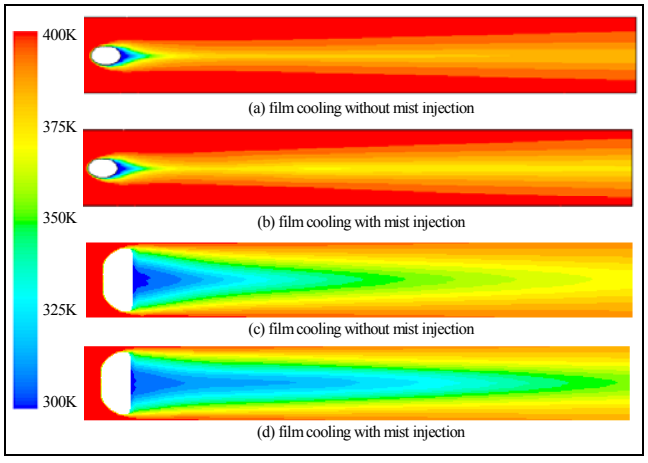

Figure 7 Wall temperature distributions of air-film cooling on the cooling surface for both round and fan-shaped holes.

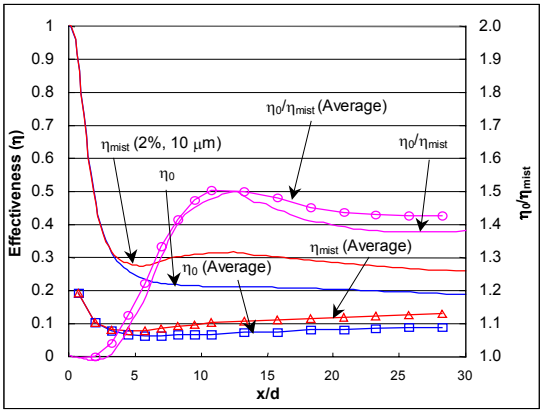

Figure 8 Centerline and spanwise average cooling effectiveness and mist cooling enhancement (round-hole)

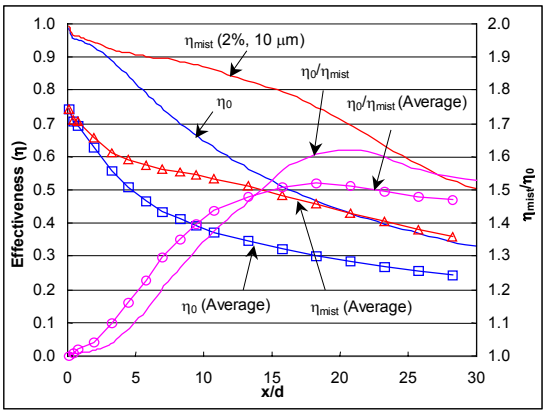

Figure 9 Centerline and spanwise average cooling effectiveness and mist cooling enhancement (fan-shaped hole)

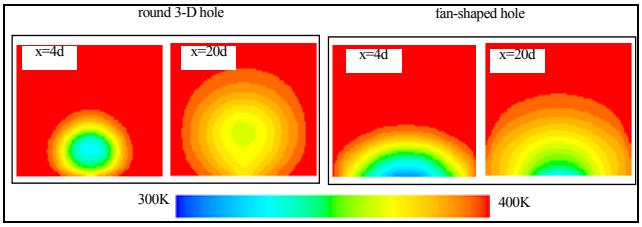

(a) Temperature distribution

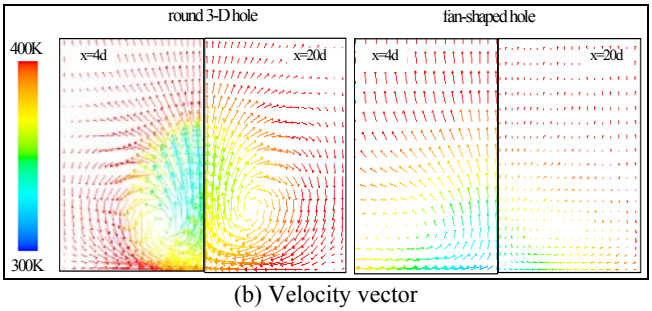

(b) Velocity vector

Figure 10 Cross-sectional temperature distributions and velocity fields in the streamwise direction (Film cooling without mist).

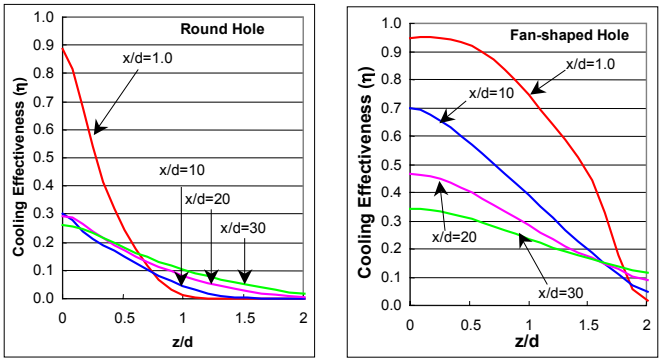

(a) Round hole (b) Fan-shaped hole

Figure 11 Spanwise distributions of cooling effectiveness for round and fan-shaped holes (Film cooling without mist).

Validation of Numerical Results - Numerical results for single-phase air film cooling are validated by comparing with data from other studies. Figure 12 shows the cooling effectiveness along the centerline of the round hole from different studies with various blowing ratios. The agreement is good in both the near and the far fields. Simulation in [7] included a plenum to account for the effect of flow inside the jet hole on film cooling, especially close to the jet exit. It has been known that the plenum geometry could affect film cooling flow pattern and cooling performance. However, under the parameters of the current study, it seems that the plenum does not play a critical role under the parameters in this study if the plenum does not induce flow separation.

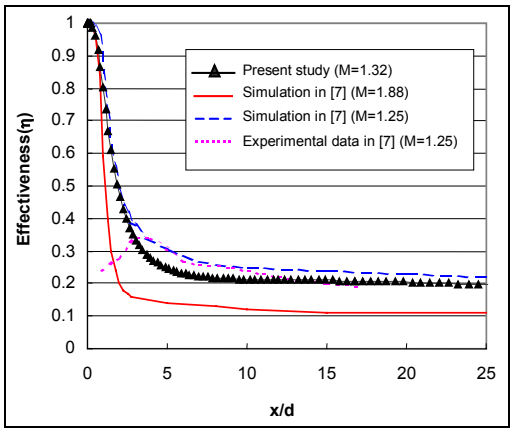

Figure 12 Comparison with other studies (Centerline cooling effectiveness of the round hole)

Effect of Mist Concentration - The effect of mist concentration is studied with a mist injection of 1, 2, and 5% of the coolant mass flow rate. Figure 13 shows the results in the 2-D slot case. It can be seen that the cooling effectiveness increases as mist concentration increases. A mist of 5% can provide a cooling enhancement of 65% at x/2b=30. The increase is about linear when the concentration is low, but it slows down at high concentration (5%) where the cooling effectiveness is close to 0.9 for the 2-D slot cooling. This high cooling effectiveness means that the temperature close to the cooling surface is low, and the droplet evaporation rate is reduced. When the mist concentration is low, higher concentration always means more latent heat is available to cool down almost the same mass of mainstream air. Therefore, a nearly linear relationship can be obtained if ignoring the effect of different main flow temperatures on evaporation. The average cooling effectiveness and mist cooling enhancement over the entire surface is listed in Table 1.

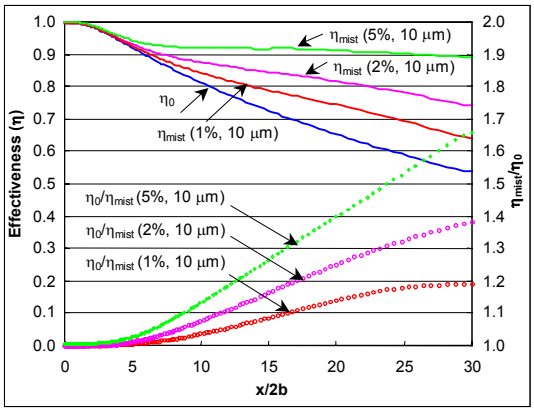

(a)

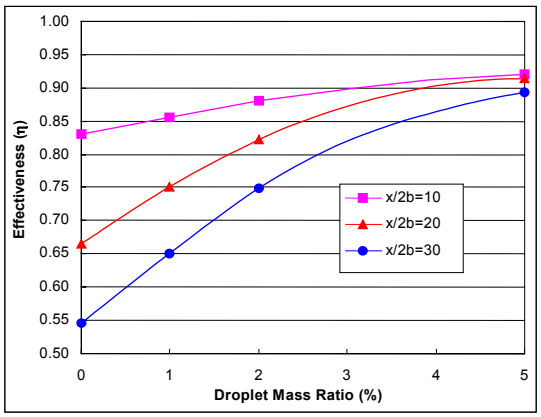

(b)

Figure 13 Effect of mist concentration on cooling effectiveness for a 2-D slot film cooling

Table 1 Cooling effectiveness and cooling enhancement averaged over the entire surface

Mist concentration (10μm)	0%	1%	2%	5%
Maximum enhancement	0	19%	38%	65%
Average effectiveness	0.747	0.804	0.855	0.925
Average η_{mist}/η_0	1	1.076	1.145	1.238

Effect of Droplet Size - The effect of droplet size on 2-D slot mist film cooling is shown in Fig. 14 for droplet sizes of 5, 10, and 20 μm, respectively. It is seen that the smaller droplets produce better cooling. Droplets of 20 μm make little difference to air film cooling, at least within the x/2b range under study. The cooling enhancement at z/2b=30 is 5% for droplets of 20 μm and the average enhancement is only 2%. The result for droplets of 50 μm shows less than 1% cooling enhancement; therefore, it goes into the same curve as the single-phase air film cooling in the figure. Notice the cooling effectiveness drops more quickly for the case with 5-μm droplets after x/2b=22 because most of the droplets have been evaporated by that time. Figure 15 shows the droplet trajectories predicted using stochastic tracking method that considers the turbulent dispersion.

The turbulent dispersion can bring the droplets towards the wall and thus improves cooling. As seen in Fig. 15, most of the 5-μm droplets evaporated before x/2b=20 while some of the 10-μm droplets can survive till the outlet. It can be concluded that a distributed size from 5 to 10 μm in real gas turbine applications will give an excellent enhancement on single-phase air film cooling. Mist film cooling can be managed by manipulating both mist concentration and the droplet size.

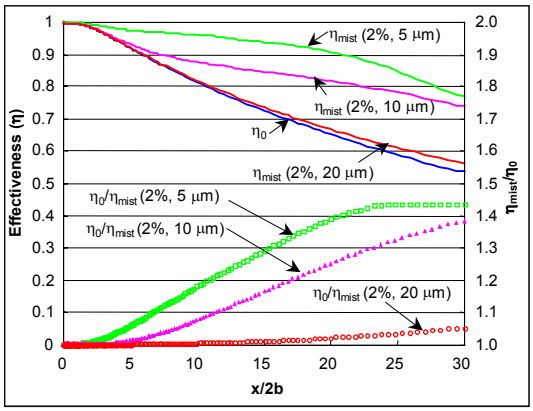

Figure 14 Effect of droplet size on cooling effectiveness for a 2-D slot film cooling.

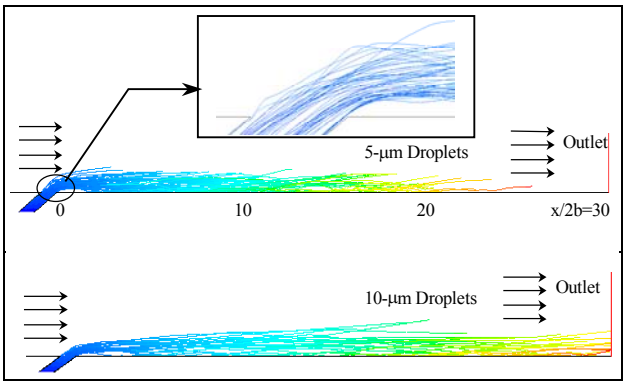

Figure 15 Droplet trajectories predicted with stochastic tracking (2-D slot case)

Effect of Blowing Ratio - To achieve the best film cooling performance, different blowing ratios might be used depending on cooling geometries and other parameters. Figure 16 shows the results with 4 different blowing ratios from 0.66 to 1.58 for 2-D slot case. To obtain different blowing ratios, the velocity of the coolant jet is changed while the mainstream flow remains the same. Mist concentration in all these cases is 2% and the droplet diameter is 10 μm. It can be seen that the single-phase cooling effectiveness itself is a function of the blowing ratio. Under the settings of the current study, the cooling effectiveness increases when the blowing ratio increases, which can be simply due to more cooling flow being provided to protect the surface. However, the enhancement of mist film cooling reduces when the blowing ratio increases. The maximum cooling enhancement at a blowing ratio of 0.66 is 52%; this value drops to 31% when the blowing ratio is 1.58. The cooing enhancements averaged over the entire surface for these two cases are 34% and 12%, respectively. This can be interpreted by the droplets moving further away from the wall at high blowing ratios. Therefore, mist film cooling performs better with smaller blowing ratios.

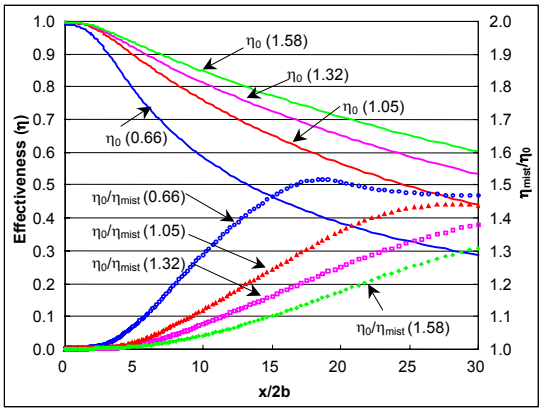

Figure 16 Effect of mist injection on the slot jet air film cooling with different blowing ratios

Effect of Blowing Angle - The effect of blowing angle on mist film cooling is shown in Fig. 17 by running 2-D slot cases. Film cooling with a 30° injection is slightly better than that with a 35° injection with and without mist. It can also be seen that the mist cooling enhancement is almost identical for these two cases although the 35° case has a little better performance, especially at x/2b>25.

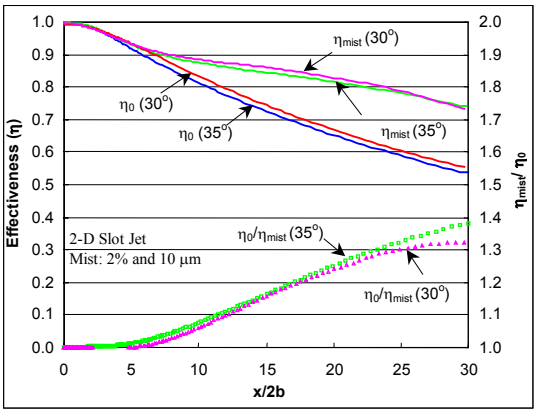

Figure 17 Effect of mist injection on the slot-jet air film cooling with different blowing angles

Effect of Main Flow Temperature - The main flow in real gas turbines is at very high temperature and pressure. Figure 18 shows the result of 2-D slot film cooling with a mainstream temperature of 500K. The blowing ratio changes from 1.3 to 1.6 due to reduced main flow density. It can be seen that dry air film cooling performs better when main flow temperature increases. The cooling with mist keeps about the same until x/2b=15~20. After that, the cooling becomes less effective than at lower main flow temperature. This can be interpreted as high-temperature mainstream absorbs more heat and makes the evaporation time shorter, and fewer droplets are left after x/2b=20. As seen in Eq. 19, higher temperature difference makes the evaporation time shorter. Increasing the mist flow rate from 2% to about 5% can make film-cooling effectiveness higher and more uniform at high mainstream temperature as shown in Fig. 18. Detailed studies are needed to explore mist film cooling in real operating conditions.

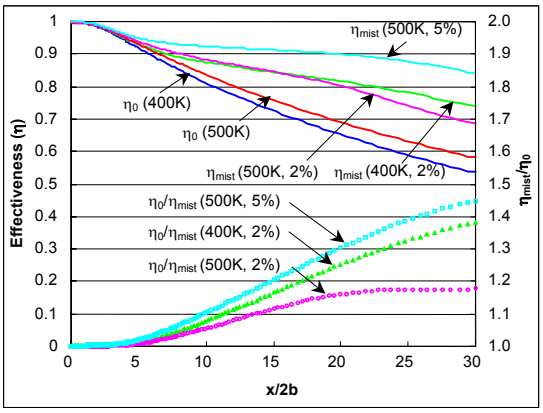

Figure 18 Effect of mist film cooling with different mainstream temperatures

Concerns and Future Research

The objective of this study is to explore the concept of mist film cooling. Numerical simulation only provides a qualitative description of the trend and effects of various parameters. Experiments are needed to verify the simulated results. In terms of the computational model, a more complicated model including heat transfer between the wall and droplets will be considered in the future. Models of collisions and coalescences will also be developed and incorporated into the future studies. Li et al. modeled the mist cooling [22] using the experimental data from [13] and reported the major contribution for mist cooling enhancement was from the direct contact between droplets and the wall. In this paper, the direct droplet-wall contact heat transfer mechanism is not included, so the cooling results could be probably 50% under predicted. More realistic conditions with high temperature and high pressure will be considered in future studies. The major reservation of applying mist film cooling from gas turbine OEMs and users is the concern related to erosion and corrosion of water droplets on the heated surface. This task will be placed upon metallurgists to find solutions.

Conclusions

Motivated to provide a significant improvement for cooling gas turbine hot section components, this paper investigates the potential of film cooling enhancement by injecting mist into the coolant. Three different holes are used, which include a 2-D slot, a round hole, and a diffusion hole. Parameter studies have been performed with 2-D slot cases. The conclusions from numerical simulation and parametric studies are:

- By injecting mist into the coolant, the performance of air film cooling can be improved significantly. Film cooling with a 2% mist can increase the cooling effectiveness about 30 ~ 50%.
- The results reveal the benefit of mist film cooling by significantly enhancing cooling downstream of x/2b (or x/d) >15, where the single-phase film cooling is less effective.
- Cooling enhancement has been shown to prevail in all three geometrical arrangements in the study. The maximum spanwise enhancement is ~50% for both the round hole jet and the fan-shaped hole jet.
- Higher mist concentration can result in higher cooling enhancement. For a 2-D slot jet, 5% mist with 10-μm droplets can provide a cooling enhancement of 65% at x/2b=30, which makes the overall cooling effectiveness reach above 0.9.
- Smaller droplets show a higher effectiveness if the concentration is high enough. Cooling enhancement drops from 43% to 5% when droplet size changes from 5 to 20 microns under the conditions studied in this paper.
- Mist film cooling performs better with smaller blowing ratio. With 2% mist, the maximum cooling enhancement can reach 52% with a blowing ratio of 0.66. The cooling effectiveness decreases as the blowing ratio increases.
- Mist cooling enhancement with a blowing angle of 30 degrees is slightly (1~2%) lower than with a blowing angle of 35 degrees at x/2b<25. The difference becomes bigger (7~8%) downstream at x/2b=30.
- Mainstream at high temperature absorbs the droplets quickly, and thus makes the cooling enhancement low. The cooling enhancement reduces from 38% to 18% when the main flow temperature increases from 400K to 500K. The low performance at high main flow temperature can be compensated by using a higher mist concentration.

Acknowledgement

This study is partially supported by the Louisiana Governor's Energy Initiative via the Clean Power and Energy Research Consortium (CPERC) and administrated by the Louisiana Board of Regents.

References

[1] Eriksen, V.L. and Goldstein, R. J., 1974, "Heat Transfer and Film Cooling Following Injection Through Inclined Tubes," ASME J. Heat Transfer, **96**, pp. 239–245.

[2] Goldstein, R. J., Eckert, E. R. G., and Burggraf, F., 1974, "Effects of Hole Geometry and Density on Three-Dimensional Film Cooling," Int. J. Heat Mass Transfer, **17**, pp. 595–607.

[3] Jia, R., Sunden, B., Miron, P., and Leger, B., 2003, "Numerical and Experimental Study of the Slot Film Cooling Jet with Various Angles," Proceedings of the ASME Summer Heat Transfer Conference, pp. 845-856.

[4] Kwak, J. S. and Han, J. C., 2003, "Heat Transfer Coefficients and Film-Cooling Effectiveness on a Gas Turbine Blade Tip," ASME J. Heat Transfer, **125,** pp. 494-502.

[5] Wang, T., Chintalapati, S., Bunker, R. S., and Lee, C. P., 2000, "Jet Mixing in a Slot," Experimental Thermal and Fluid Science, **22**, n. 1, pp. 1-17.

[6] Bell, C. M., Hamakawa1, H., and Ligrani, P. M., 2000, "Film Cooling From Shaped Holes," ASME J. Heat Transfer, **122,** pp. 224-232.

[7] Brittingham, R.A. and Leylek, J. H, 2002, "A Detailed Analysis of Film Cooling Physics: Part IV—Compound-Angle Injection with Shaped Holes," ASME J. Turbomachinery, **122,** pp. 133-145.

[8] Chaker, M., Meher-Homji, C.B., and Mee, M., 2002, "Inlet Fogging of Gas Turbine Engines - Part A: Fog Droplet Thermodynamics, Heat Transfer and Practical Considerations," ASME Proceedings of Turbo Expo 2002*,* **4**, pp. 413-428.

[9] Petr, V., 2003, "Analysis of Wet Compression in GT's," Energy and the Environment - Proceedings of the International Conference on Energy and the Environment, **1**, pp. 489-494.

[10] Nirmalan, N. V., Weaver, J. A., and Hylton, L. D., 1998, "An Experimental Study of Turbine Vane Heat Transfer with Water–Air Cooling," ASME J. Turbomachinery, **120**, No. 1, pp. 50–62.
[11] Guo, T., Wang, T., and Gaddis, J. L., 2000, "Mist/Steam Cooling in a Heated Horizontal Tube, Part 1: Experimental System, Part 2: Results and Modeling," ASME J. Turbomachinery, **122**, pp. 360–374.
[12] Guo, T., Wang, T., and Gaddis, J.L., 2001, "Mist/Steam Cooling in a 180^o Tube Bend," ASME J. Heat Transfer, **122,** pp. 749-756.
[13] Li, X., Gaddis, J. L., and Wang, T., 2003, "Mist/Steam Cooling by a Row of Impinging Jets," Int. J. Heat Mass Transfer, **46**, pp. 2279-2290.
[14] Li, X, Gaddis, J. L., and Wang, T, " Mist/Steam Heat Transfer with Jet Impingement onto a Concave Surface," ASME J. Heat Transfer, vol. 125, pp. 438-446
[15] Dittmar, J., Schulz, A., and Wittig, S., 2003, "Assessment of Various Film-cooling Configurations Including Shaped and Compound Angle Holes Based on Large-scale Experiments," ASME J. Turbomachinery, **125**, n. 1, pp. 57-64.
[16] Fluent Manual, Version 6.1.22, 2003, Fluent, Inc.
[17] Launder, B. E. and Spalding, D. B., 1972, Lectures in Mathematical Models of Turbulence*,* Academic Press, London, England.
[18] Wolfstein, M., 1969, "The Velocity and Temperature Distribution of One-Dimensional Flow with Turbulence Augmentation and Pressure Gradient," Int. J. Heat Mass Transfer, **12,** pp. 301-318.
[19] Ranz, W. E. and Marshall, W. R. Jr., 1952, "Evaporation from Drops, Part I," Chem. Eng. Prog., **48**, pp. 141-146.
[20] Ranz, W. E. and Marshall, W. R. Jr., 1952, "Evaporation from Drops, Part II," Chem. Eng. Prog., **48**, pp. 173-180.
[21] Kuo, K. Y., 1986*,* Principles of Combustion, John Wiley and Sons, New York.
[22] Li, X., Gaddis, J. L., and Wang, T., 2001, "Modeling of Heat Transfer in a Mist/Steam Impinging Jet," ASME J. Heat Transfer, **123**, pp. 1086-1092.